

RSC Advances



This is an *Accepted Manuscript*, which has been through the Royal Society of Chemistry peer review process and has been accepted for publication.

Accepted Manuscripts are published online shortly after acceptance, before technical editing, formatting and proof reading. Using this free service, authors can make their results available to the community, in citable form, before we publish the edited article. This *Accepted Manuscript* will be replaced by the edited, formatted and paginated article as soon as this is available.

You can find more information about *Accepted Manuscripts* in the [Information for Authors](#).

Please note that technical editing may introduce minor changes to the text and/or graphics, which may alter content. The journal's standard [Terms & Conditions](#) and the [Ethical guidelines](#) still apply. In no event shall the Royal Society of Chemistry be held responsible for any errors or omissions in this *Accepted Manuscript* or any consequences arising from the use of any information it contains.



Journal Name

ARTICLE

One-pot Synthesis of Multidimensional Conducting Polymer Nanotubes for Superior Performance Field-Effect Transistor-Type Carcinoembryonic Antigen Biosensors

Received 00th January 20xx,
Accepted 00th January 20xx

DOI: 10.1039/x0xx00000x

www.rsc.org/

Jin Wook Park, Wonjoo Na, and Jyongsik Jang*

Carcinoembryonic antigen (CEA), as one of the glycoprotein, is crucially important tumor marker due to related to a sort of carcinomas. Abnormal level of CEA in the serum is connected to diagnosis of cancer. In this work, highly sensitive and selective field-effect transistor (FET) biosensors were fabricated to detect CEA, using aptamer-functionalized multidimensional conducting-polymer (3-carboxylate polypyrrole) nanotubes (Apt-C-PPy MNTs). The multidimensional system, C-PPy MNTs, is firstly produced by solution based temperature controlled self-degradation method. The C-PPy MNTs are integrated with the CEA-binding aptamer immobilized on the interdigitated array electrode substrate by covalent bonding with amide groups (-CONH) to produce a FET-type biosensor transducer. The resulting C-PPy MNT-based FET sensors exhibit a rapid response in real time (<1 s), ultrasensitivity toward CEA with a limit of detection of 1 fg mL⁻¹. This limit of detection is 2–3 orders of magnitude more sensitive than previous reports. The liquid-gated FET-type sensor showed specificity toward CEA in a mixed solution containing compounds found in the similar proteins and biological signals. Additionally, a superior lifetime is demonstrated for the FET sensor, owing to the covalent bonding involved in the immobilization processes.

Introduction

Carcinoembryonic antigen (CEA) is a glycoprotein that has been widely regarded as one of the most important tumor markers. CEA is associated with a number of carcinomas, including lung cancer, breast cancer and rectal cancer.^[1–3] Serum CEA levels in cancer patients are usually significantly higher than those found in healthy people; therefore, accurate determination of CEA levels can contribute to cancer diagnosis and treatment. The development of CEA sensing methods with high sensitivity and specificity has been an important research goal in recent years. A number of protocols have been proposed for CEA detection, including an enzyme-linked immunosorbent assay,^[4–6] piezoelectric device,^[7] surface plasmon resonance,^[8] radioimmunoassay,^[9–11] magnetoimpedance,^[12] electroluminescence immunoassay,^[13] fluorometric,^[14] and electrochemical analysis.^[15–17] Although existing methods have been successful, it is necessary to improve the sensitivity and simplicity of existing CEA assays. The most commonly used immunoreaction-based sensors are able to provide good reliability. However, they are in principle heterogeneous and involve multiple steps and time-consuming procedures. In addition, higher sensible and more accurate CEA sensor devices are demanded to use in the practical application. Field-effect transistors (FETs) have attracted

interest as candidates to fabricate state-of-the-art sensor platforms owing to their capability of achieving high current amplification while maintaining an increased signal-to-noise ratio.^[18–23] In particular, one-dimensional (1D) nanomaterials that show superior charge carrier mobility along the long-axis can be employed for use in highly sensitive sensors.^[24–28] In recent decades, immense effort has been devoted to the fabrication of various 1D nanostructures. For example, metallic and ceramic nanostructures have been fabricated extensively. Their nanometer- and atomic-scaled structures can be precisely controlled using,^[29] such as chemical vapor deposition,^[30–31] or colloidal synthesis.^[32–33] Additionally, unique size- and shape-dependent properties have been characterized in such inorganic nanomaterials. However, it is difficult to functionalize the surface of the inorganic nanostructures for attaching specific protein or DNA acceptors as biological signals for use in biosensor applications. Recently, the fabrication technology of 1D conducting polymers (CPs) at the nanometer scale has been actively investigated due to their unique optical, electrical and mechanical properties.^[34–36] In particular, 1D CP nanomaterials exhibit a number of advantages for use in biosensing applications, including easy functionalization and biocompatibility.^[37–40] These 1D CP nanostructures were fabricated using vapor methods (e.g., oxidative chemical vapor deposition),^[41–44] solutions (e.g., micelle templating) phase synthesis,^[45–46] and self-degradation synthetic methods.^[47–48] Recently, unique 1D CP nanotube (NT) structures, consisting of nanowires and nanonodules grown on the surface, were developed by vapor deposition polymerization and etching processes.^[49–50] These unique structures exhibited an improved surface-to-volume ratio with an anisotropic tubular structure that provided efficient charge carrier transport along the rotational axis of the NT, and

School of Chemical and Biological Engineering,
Seoul National University, 599 Gwanangno, Gwanakgu, Seoul 151-742, Korea
E-mail: jsjang@plaza.snu.ac.kr; Fax: +82 2 880 1604; Tel: +82 2 880 7069

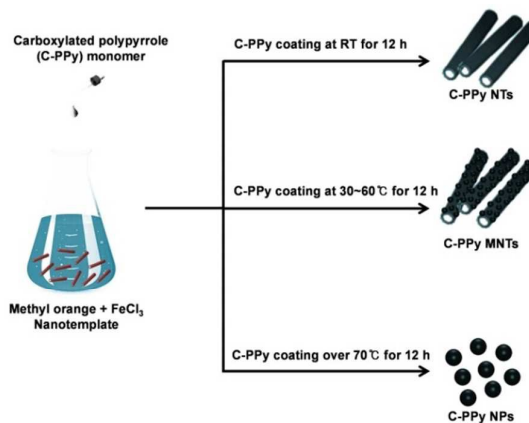
*Electronic Supplementary Information (ESI) available: Photoimages, TEM, FE-SEM and Raman spectra of samples. Electrochemical-properties of samples were described. See DOI: 10.1039/x0xx00000x

reactive binding sites between the analyte and transducer in biosensor applications. However, the processes required multiple steps with time-consuming procedures and expensive equipment (e.g., electro-spinning technology), and are difficult to fabricate in large-scale production.

Here, we describe fabrication of a FET-type aptamer sensor to detect CEA based on the carboxylated polypyrrole multidimensional nanotubes (C-PPy MNTs) conjugated with a CEA-binding aptamer. **Scheme 1** illustrates the overall procedure for fabrication of C-PPy MNTs. This is a facile, efficient, and cost-effective method for large-scale production of multidimensional CP NT structures, using simple aqueous solution-based temperature-controlled synthesis. The surface area of the C-PPy MNTs is three to four times larger than that of pristine C-PPy NTs, due to the formation of nano-protuberances on the surface of the pristine NTs. As a result, the interaction between the analyte and C-PPy MNTs-based transducer is enhanced. Anchoring C-PPy MNTs on the electrode surface and immobilization of the CEA-binding aptamer enables a strong affinity between the aptamer and CEA in an aptamer-FET platform suitable for electronic control. The real-time response of liquid-ion-gated FET-type aptasensors based on C-PPy MNTs to CEA was particularly rapid (<1 s). The intensity of the response increased with increasing CEA concentration, and the detection limit was approximately 1 fg mL^{-1} , which is about 2–3 orders of magnitude lower than the lowest previously reported detection limit for an CEA sensor system. Furthermore, a high degree of specificity and reusability over a long time toward CEA was observed. To the best of our knowledge, this is the first experimental demonstration of a FET-type CEA-aptasensor using C-PPy MNTs as signal transducers.

Results and discussion

The morphology of the C-PPy nanostructures was investigated using scanning electron microscopy (SEM) and transmission electron microscopy (TEM). **Fig. 1a** shows SEM and TEM images of the pristine C-PPy NTs, revealing that the diameter of the tubes was around 70 nm. Increasing numbers of nano-protuberances were observed on the surface of the C-PPy NTs with increasing reaction temperature, leading to the formation of C-PPy MNTs (see **Fig. 1b-e**). The temporary self-assembled nano-template was initially fabricated through electrostatic interaction between methyl orange (MO) and ferric chloride under solution, and the ferric ions were adsorbed on the surface of the template. With increasing reaction temperature, ferric ions and MO were randomly dispersed under solution and self-assembled structures emerged due to electrostatic interactions. These self-assembled structures formed nano-protuberance shapes that were grown and aggregated on the surface of the nanotube, resulting in the construction of multidimensional NT structures. The number and size of the nano-protuberances on the surface of the C-PPy NTs increased as temperatures increased over 40°C . After injecting liquid monomer into the solution, chemical polymerization proceeded on the ferric ions adsorbed on the nanotemplate surface, which resulted in the formation of a polymer sheath on the nanotemplate. The



Scheme 1 Illustrative diagram of the fabrication method for polypyrrole-3-carboxylated multidimensional nanotubes (C-PPy MNTs).

nanotemplate was removed by excess solution and vigorous stirring. In contrast, the CP nanostructures have strong interchain - interactions, and do not dissolve under solution. Thus, the core nanotemplate was readily etched without structural deformation of the C-PPy shell, resulting in the formation of the MNT structures. However, the NT structures were destroyed and reformed to a nanoparticle (NP) shape at temperatures over 70°C , as shown in **Fig. 1f**. In this article, we focus on the MNT structures for a FET-type biosensor application because NP structures were poorly characterized due to their densely aggregated state. To the best of our knowledge, there are no previous studies on the fabrication of these unique multidimensional CP nanostructures using a one-pot solution-based synthetic method. This synthetic method has a number of advantages such as simple, easy fabrication, and the potential for large-scale production. Chemical characterization of the C-PPy MNT structures was carried out using attenuated total reflectance (ATR) Fourier transform infrared (FTIR) spectroscopy, as shown in **Fig. 2a**. The FTIR spectrum of the PPy MNTs did not show carbonyl and hydroxyl group peaks. In contrast, the C-PPy MNTs spectrum exhibited a carboxylic acid stretching peak at 1733 cm^{-1} , a pyrrole ring stretching peak at 1554 and 1475 cm^{-1} , and a C-N stretching peak at 1294 cm^{-1} .^[51–52] This result suggests that C-PPy MNTs were successfully synthesized using the temperature controlled one-pot solution synthetic method.

The X-ray diffraction diffractograms of the C-PPy NTs showed a broad peak at around 2θ ($d = 3.56$), corresponding to the pyrrole intermolecular distance, as shown in **Fig. 2b**.^[51–52] The C-PPy MNTs showed a similar and slightly shifted shape due to the formation of nano-protuberances on the surface of the NTs. These results suggest that the C-PPy MNTs are composed of amorphous polymer structures and were successfully synthesized.

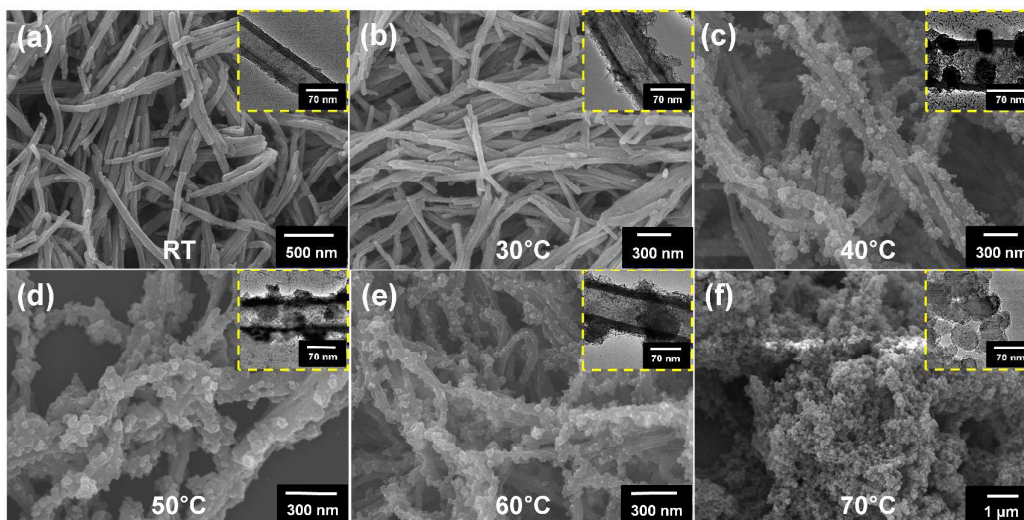


Fig. 1 SEM and TEM images of the C-PPy nanostructures based on different controlled temperatures of the synthesis method. (a: room temperature (RT), b: 30°C, c: 40°C, d: 50°C, e: 60°C, f: 70°C)

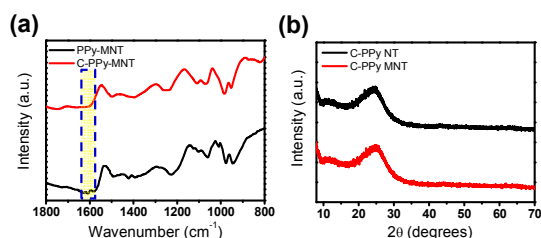


Fig. 2 (a) ATR-FT-IR and (b) XRD spectra of C-PPy NTs and C-PPy MNTs.

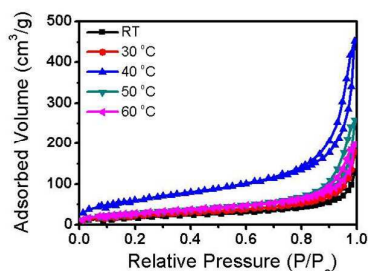


Fig. 3 N₂ adsorption/desorption isotherms of various temperature controlled C-PPy MNTs.

To investigate the characteristics of the multidimensional nanostructures, Brunauer–Emmett–Teller (BET) measurements were conducted, as shown in **Fig. 3**. The specific surface area of the MNTs ($166\text{--}376\text{ m}^2\text{ g}^{-1}$) is much higher than that of a pure NT structure ($100\text{ m}^2\text{ g}^{-1}$). The nano-protuberances on the surface of the C-PPy NT lead to an enhanced surface-to-volume ratio, improving the specific surface area. However, when the reaction temperature exceeds 40°C , the size of the C-PPy NTs and nano-protuberances increases, leading to a smaller specific surface area

($40^\circ\text{C} = 376\text{ m}^2\text{ g}^{-1}$, $50 = 352\text{ m}^2\text{ g}^{-1}$, $60^\circ\text{C} = 314\text{ m}^2\text{ g}^{-1}$). This result suggests that the high kinetic energy of the nano-protuberances induces dense aggregation and a growth in size due to fast, unstable, active diffusion under solution. Thus, the highest surface area is found in the MNT structures grown at a temperature of 40°C .

To fabricate highly sensitive FET biosensor electrode, the stability of the sensing environment in the liquid-ion solution is crucial factor. We introduced the covalent bonding of functional groups for the immobilization of the transducer on the sensor electrode with the binding receptor on the transducer to enhance stability. The procedure for the immobilization of the aptamer-conjugated C-PPy on the electrode substrate is described as shown in **Fig. 4**. Firstly, an interdigitated microelectrode array (IDA) was patterned on a glass substrate using a lithographic process, composed of pairs of 25 lines of gold fingers on the glass plate. To functionalize the surface with amine groups ($-\text{NH}_2$), the IDA glass substrate was treated with 3-aminopropyltrimethoxysilane (APS). Then, the condensation reaction between carboxyl group ($-\text{COOH}$) of the MNTs and APS-treated electrode formed amide bonding ($-\text{CONH}$), using the condensing agent 4-(4,6-dimethoxy-1,3,5-triazin-2-yl)-4-methylmorpholinium chloride (DMT-MM). Thus, the C-PPy MNTs were covalently anchored on the IDA electrode via simple condensation reactions. The carboxyl group of the C-PPy MNTs facilitated the attachment of the binding aptamers to the tube surface. A similar condensation reaction was found between the carboxyl group of the C-PPy MNTs and the amino group of the CEA binding aptamer using a condensing agent (DMT-MM). Therefore, the CEA-aptamer IDA biosensor electrode was fabricated based on the aptamer-conjugated C-PPy MNTs (Apt-C-PPy MNTs), and demonstrated outstanding stability against environmental perturbation.

To investigate the electrical characteristics of the Apt-C-PPy MNTs in the liquid phase, a FET configuration was constructed using a liquid-ion gate. **Fig. 5a** shows the Current–voltage (I – V) characteristics of the C-PPy MNTs from NTs grown at different temperatures, before immobilization of the CEA-binding aptamer. All of the C-PPy MNTs with no aptamer conjugation showed linearity (i.e., an ohmic contact) for voltages ranging from -0.2 to 0.2 V , as opposed to the nonlinearity exhibited by Schottky barriers

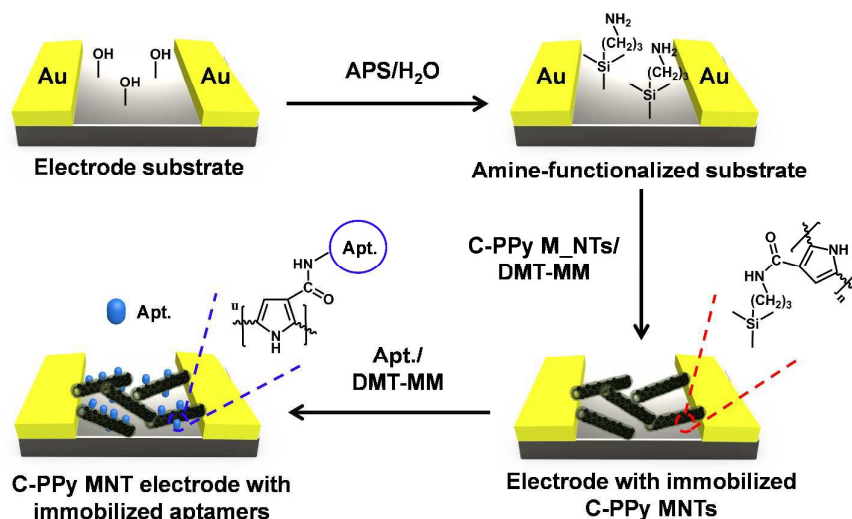


Fig. 4 Schematic diagram of the immobilization process used to produce the sensor electrode based on aptamer-conjugated C-PPy MNTs (Apt-C-PPy MNTs) on the IDA electrode substrate. Apt. represents aptamer.

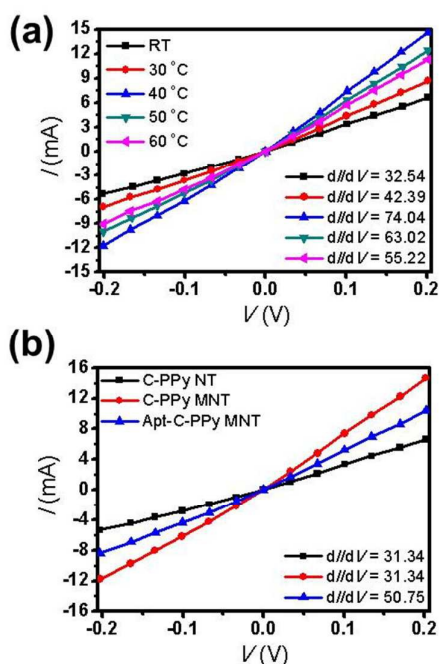


Fig. 5 Source-drain current voltage (I_{SD} - V_{SD}) curve comparison of the I_{DA} electrodes based on (a) various temperature controlled C-PPy MNTs and (b) C-PPy NT, C-PPy MNT, and Apt-C-PPy MNTs for a V_{SD} scan rate of 40 mV s^{-1} .

with poor electrical contact at the electrode. The excellent conductivity was found on the C-PPy MNTs grown at 40°C . Interestingly, this result is similar tendency of the BET data, because the C-PPy MNTs with higher surface area have more dense and effective conjugated structures.^[49-50] Thus, we conclude that the MNT structures provided more efficient charge carrier transport along the rotational axis of the NT than that of the NT structures.

Fig. 5b shows the I-V characteristics of the C-PPy MNTs, before and after immobilization of the CEA-binding aptamer. After the binding aptamer became immobilized on the NT surface, the dI/dV values of the electrode decreased. This result is deduced that the oxidation level of C-PPy MNTs changed during aptamer introduction, because of the detachment of doped elements via condensation reaction. Nevertheless, the dI/dV value and linearity maintained with the same order of magnitude after aptamer immobilization. These results suggested that the binding aptamer was effectively incorporated into the C-PPy MNTs with no deterioration in electrical contact. Additionally, compared to pristine C-PPy NTs, the electrical properties of the C-PPy MNTs exhibited higher conductivity, due to the enhanced contact area with the electrode substrate, arising from the presence of nano-protuberances on the tube surface. A schematic diagram of the Apt-C-PPy MNT FET-sensor platform was shown in Fig. 6a. The FET sensor platform was surrounded with phosphate-buffered saline (PBS) at 7.4 as the electrolyte. The two gold IDA bands acted as the source (S) and drain (D) in the FET-type sensor system. The gate potential (V_G) was applied to the source electrode through a buffer solution. The charge transport properties of Apt-C-PPy MNTs in the FET configuration were tested through the source-drain current (I_{SD}) values on V_G in the range -0.9 to 0.5 V at a constant source-drain voltage scan rate of 0.2 V s^{-1} . Fig. 6b exhibits a plot of I_{SD} versus V_{SD} for varying V_G based on the Apt-C-PPy MNT FET-sensor device. The I_{SD} increased (i.e., became more positive) when a larger negative gate bias was applied. This result indicates p-type (hole-transport) behavior, caused by an increase in the oxidation level of the polymer chains.^[22] This is typical of CP transistor performance. Consequently, this result shows Apt-C-PPy MNT FETs could be used effectively as an electrochemical biosensor for detecting analytes in a PBS buffer solution. The liquid-ion gate has ability to increase transconductance, owing to the close contact between the Apt-C-PPy MNTs and the gate compared with conventional backgating.

To investigate the sensing performance of the liquid-ion-gated Apt-C-PPy MNT FET, I_{SD} changes were measured in real time with a

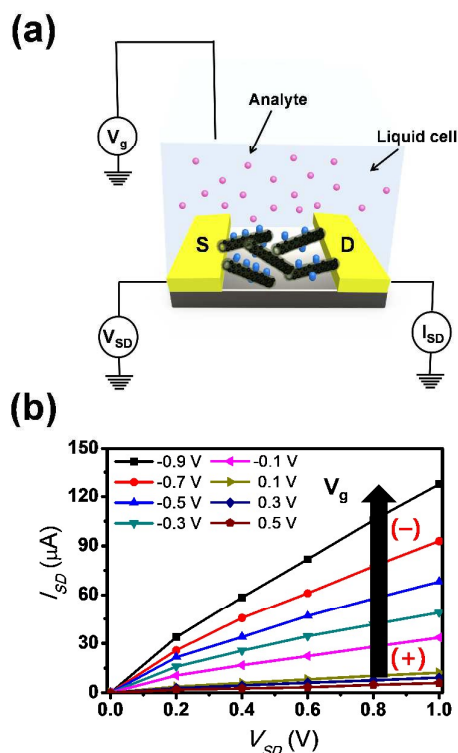


Fig. 6 (a) Schematic diagram of liquid-ion-gated FET with the Apt-C-PPy MNT array. (b) Source-drain current versus source-drain voltage (I_{SD} - V_{SD}) characteristics of an Apt-C-PPy MNT FET electrode for a varying gate voltage (V_G) ranging from -0.9 to 0.5 V in -0.2 V steps (V_{SD} scan rate: 0.2 V s^{-1}).

V_G of -0.1 V ($V_{SD} = 0.1$ V), a low operating voltage, upon the addition of various concentrations of CEA.

The C-PPy MNTs were studied based on the 40°C synthesis condition because this has the highest specific surface area and best electrical properties, and is expected to provide the best sensing performance. Fig. 7a shows the real-time response of the Apt-C-PPy MNT and Apt-C-PPy NT FET sensors as a function of CEA concentration. Upon each CEA addition, I_{SD} increased rapidly over a 1-s period before reaching its saturated value. The dependence of the conductance on gate voltage makes FETs natural candidates for electrically based sensing platform because the electric field resulting from binding of a charged species to the gate dielectric is analogous to applying a voltage using a gate electrode. Specifically, the FET-type CEA Apt-C-PPy MNT can be operated using an electrostatic gating effect. Thus, the CEA-aptamer binding events can effectively induce negative point charges in the liquid-ion gate dielectric near the C-PPy MNT surface, accumulating positive charge carriers in the C-PPy MNT channels. The reinforced negative gate voltage effect from the CEA-aptamer interaction resulted in increased current (I_{SD}) for the p-type C-PPy MNTs. This is similar to a p-type doping effect acting indirectly on the liquid-ion gate dielectric, rather than directly affecting the semiconducting layer. From this sensing mechanism, the intercalated close-packed C-PPy MNT arrays can elicit an enhanced charge separation by polarons or polaritons of the conducting polymer, thus providing a fast and efficient electronic pathway between the C-PPy MNT and the bound CEA-aptamer. The sensitivity of the Apt-C-PPy MNT

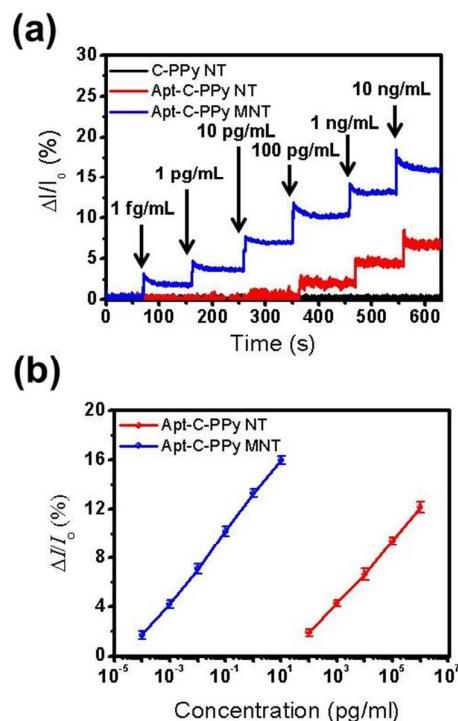


Fig. 7 Real-time response for the FETs comprising C-PPy MNT FET, Apt-C-PPy NT FET and Apt-C-PPy MNT FET, with normalized current changes, (b) Calibration curves of FETs comprising Apt-C-PPy NT FET and Apt-C-PPy MNT FET as a function of CEA concentration. ($V_G = -0.1$ V, $V_{SD} = 0.1$ V).

FETs was greater than that of the pure Apt-C-PPy NT FET; that is, the Apt-C-PPy MNT FET was capable of detecting CEA concentrations as low as 1 fg/mL at room temperature. The Apt-C-PPy MNT structures have a higher density of chemical functionality (degree of carboxylic acid group and aptamer introduced), compared to Apt-C-PPy NTs; therefore, a better sensitivity was achieved with Apt-C-PPy MNT as a result of the enhanced aptamer-CEA interaction. As a control experiment, an identical test was performed with the pristine C-PPy NTs: no significant current signals were observed. Although both Apt-C-PPy MNT and Apt-C-PPy NT FETs were sensitive to the specific CEA, the minimum detectable level was clearly different: that of the Apt-C-PPy MNT (1 fg mL^{-1}) FET sensor was 1,000 times higher than that (100 pg mL^{-1}) of Apt-C-PPy NTs. Notably, Apt-C-PPy MNTs had the lowest detection limit of 1 fg mL^{-1} (signal-to-noise ratio: 3.2), which is two to three orders of magnitude more sensitive than previously reported optoelectronic and electrochemical CEA sensors, as shown in Table 1.

Fig. 7b shows changes in sensitivity as a function of structure shape with respect to CEA concentration. The sensitivity was determined from the saturation point of the normalized current change ($(\Delta I/I_0)_{SD} \times 100$), measured 10 s after CEA addition. Compared to CEA sensors based on pristine C-PPy NTs, the C-PPy MNTs showed three fold higher sensitivity. Importantly, the sensitivity of the C-PPy MNT electrode was higher than that of the C-PPy NTs, due to the enhancement of the active functional sites on its surface and electrical performance. The CEA selectivity of the Apt-C-PPy MNT FET was investigated by real-time monitoring of I_{SD}

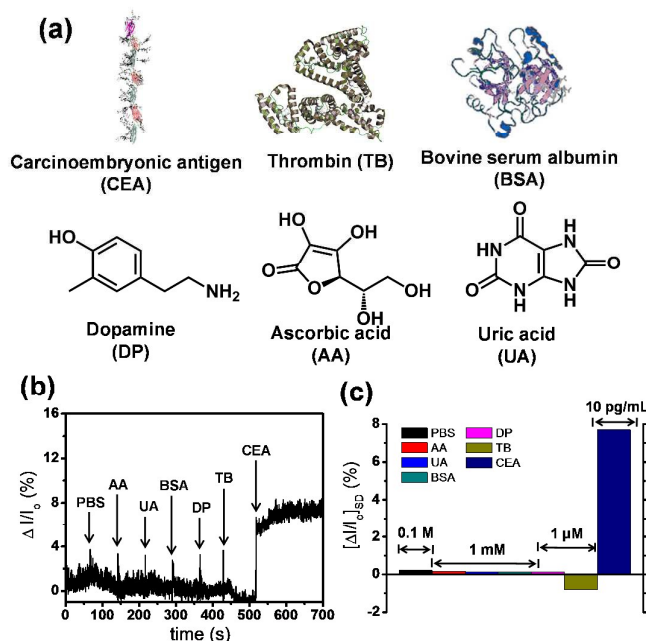


Fig. 8 (a) Molecular diagram of the CEA, TB, BAS, DP, AA and UA. (b) Selectivity responses of the aptamer sensor using the Apt-C-PPy MNTs toward non-target (PBS, AA, UA, BSA, DP, TB) and target (CEA) analytes. (c) A histogram detailing the sensing performance of the Apt-C-PPy MNTs to PBS, AA, UA, BSA, DP, TB, and CEA.

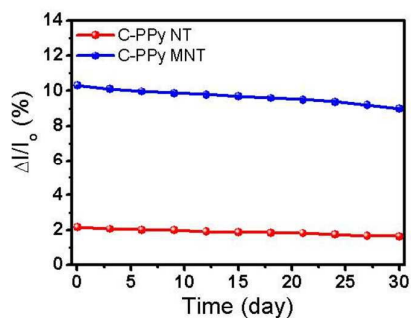


Fig. 9 Comparison of the sensing performances of Apt-C-PPy NT and Apt-C-PPy MNT FET sensors after 4 weeks of storage. Measurements were obtained at 3 day intervals.

for several related proteins and biological interfering agents: PBS, thrombin (TB), bovine serum albumin (BSA), dopamine (DP), ascorbic acid (AA) and uric acid (UA) (Fig. 8a-b). The Apt-C-PPy MNT sensor showed no significant I_{SD} changes with the addition of each non-target analyte (0.2 M: PBS; 1 mM: AA, UA, HSA; 1 μ M: DP, TB); however, considerable I_{SD} changes were evident upon the addition of 10 pg/mL CEA. A remarkable increase in current occurred when CEA was injected, even at far lower concentrations than the other compounds in the analyte, as shown in Fig. 8c. Thus, the Apt-C-PPy MNT FET sensor showed a high selectivity for CEA. Furthermore, the chemical-bonding-based FET biosensor system has the possibility of repeated use (i.e., longer lifetime and cycle stability) compared with adsorption-based system. Fig. 9 shows an estimation of the stability of the FETs based on Apt-C-PPy NTs and

Apt-C-PPy NTs over several weeks at a constant concentration (100 μ g mL⁻¹). The Apt-C-PPy MNT FETs were rinsed with distilled water and stored in a sealed vessel at 25°C under air-dried conditions for removing the residues. We injected the CEA concentration of 100 μ g mL⁻¹ several times at an injection interval of 3 days. After 4 weeks, the I_{SD} decreased to ca. 16% (22% for the system originating from Apt-C-PPy NT FETs). This decrease in sensitivity was attributed to the inactivation of the binding aptamer or the destruction of the C-PPy MNT array. The covalent anchoring between the Apt-C-PPy MNTs and electrode substrate provided superior stability for long-term reusability. Thus, this Apt-C-PPy MNT FET-biosensor could be reused in consecutive assays.

Conclusions

We demonstrated high sensitivity and specificity toward CEA using a liquid-ion-gated FET sensor based on Apt-C-PPy MNTs. The Apt-C-PPy MNTs were fabricated via solution-based temperature-controlled self-degradation method, immobilized on the electrode surface, and bonded to the amine-modified CEA binding aptamer through amide covalent bonding. The fabricated FET sensor exhibited p-channel behavior, with good electrical conductivity, and Ohmic contacts were formed with the source and drain electrodes. To the best of our knowledge, this is the first demonstration of a multidimensional CP NTs-based FET-type CEA aptamer sensor. The Apt-C-PPy MNT FET sensors showed ultra-high sensitivity (~ 1 fg mL⁻¹) to CEA, 10^2 – 10^3 times higher than that of other previous reported sensors. Additionally, the Apt-C-PPy MNT FET sensor displayed not only specific selectivity to CEA, but also highly reproducible and reusable over a long period (4 weeks in this study), due to the covalent bonding used in the immobilization process for sensing. Thus, these FET-type CEA biosensors based on Apt-C-PPy

Table 1 Comparison of the performance of various CEA sensors.

Biosensor configuration	Detection limit (pg mL ⁻¹)	Reference
UCP/CNP FRET	1000	[53]
Graphene/Au electrode	280	[54]
TH-doped Au NPs ELISA	10	[6]
Ag/Au coated graphene sensor	8	[55]
AuNP/AuNC SEF	3	[56]
HRCA colorimetry	2	[57]
QD CE-CL	8	[58]
QD/GO APCE	5	[59]
Si NW FET-type sensor	0.9	[60]
BA-DNA enzyme EC sensor	0.5	[61]
Au/Pd C-S NP EC sensor	0.4	[62]
MoS ₂ /Au/Ag NP EC sensor	0.27	[63]
RGO-Au NP/QD PEC	0.47	[64]
C-PPy MNT FET-type sensor	0.0001	This work

UCP = upconversion phosphors, CNP = carbon nano particle, FRET = fluorescence resonance energy transfer, TH = Thionine, NP = Nanoparticle, ELISA = enzyme linked immunosorbent assay, NC = Nanocluster, SEF = surface-enhanced fluorescence, HRCA = hyperbranched rolling circle amplification, CE-CL = electrophoresis-chemiluminescence, QD = quantum dot, GO = graphene oxide, PEC = photoelectrochemical system, EC = electrochemical system, C-S = Core-shell, RGO = reduced graphene oxide

MNTs can be effectively used and applicable over a wide range of applications in biological and environmental research.

Experimental section

Materials : Pyrrole (98%), pyrrole-3-carboxylic acid (P3CA), UA, (AA, TB, BSA, dopamine, DP, MO, DMT-MM, iron chloride (FeCl₃, 97%) and CEA (> 95% from human fluids) were purchased from Sigma-Aldrich Co. (St. Louis, MO, USA) and used without further purification. The CEA binding aptamer was from Bioneer Co. (Dajeon, Korea). The CEA binding aptamer was modified at the 5' terminus with an amine group, and its sequence was as follows: 5'-NH₂-(CH₂)₆-ATA CCA GCT TAT TCA ATT-3'.

Synthesis of C-PPy MNTs: The C-PPy NTs were first fabricated using a self-degraded template method, whereby 1.5 mmol FeCl₃ (0.243 g) was added to a 5 mM solution of sodium 4-[4'-(dimethylamino)phenyldiazo]phenylsulfonate, methyl orange, (0.05 g) in deionized water. After a red-colored precipitate appeared, 0.05 mM of P3CA (0.006 g) and 1.5 mM of pyrrole (0.1 g) monomer solution were added. and the mixture was stirred at RT for 18 hr. The resulting precipitate was purified by washing with deionized water and ethanol several times until the filtrate was colorless and had a neutral pH; 0.08 g of powdered CPPyNTs, with 79.5% purity, was obtained then dried under vacuum at 60 °C for 12 hours. C-PPy MNTs made at 30, 40, 50, 60, and 70°C were prepared using the same method.

Fabrication of CPPyNT-aptamer FET sensor: The IDA substrate was patterned using a photolithographic process. A microarray of 80 pairs of Au interdigitated microelectrodes on a glass substrate using a 50 nm-thick Cr adhesion layer was patterned and the resulting electrodes were obtained formed on a 50 nm-thick, 10 μm-wide, and 4 mm-long Au-Cr layer with 10 μm interelectrode spacing. To construct the CPPyNT-aptamer FET sensor platform, the IDA electrode was first treated with 5 wt% aqueous APTES for 6 h to introduce amino groups onto the substrate. Then, a mixture of 1 wt% of CPPyNT (10 μL) in water and 1 wt% aqueous DMT-MM (10

μL) was dropped onto the electrodes. Subsequently, the coupling reaction to attach the CEA binding aptamer to the CPPyNT surface was carried out using a mixture of 1 μM of CEA binding aptamer and 1 wt % aqueous DMT-MM (10 μL) for 12 hr. The FET sensor substrate based on a liquid-ion gate was fabricated with PBS, with a pH of 7.5. The current was monitored at room temperature using a source meter device.

Instrumentation: High-resolution TEMs were obtained using a JEM-3100 (JEOL, Ltd., Tokyo, Japan) at the National Center for Inter-University Research Facilities at Seoul National University. For TEM measurements, samples were diluted in ethanol and deposited onto a copper grid coated with a carbon film. Field emission SEMs were obtained using a JSM-6700F (JEOL). Specimens were coated with a thin layer of gold to eliminate charging effects. Raman spectra were recorded using a Horiba Jobin Yvon T64000 (Horiba, Ltd., Kyoto, Japan). ATR-FTIR spectra were collected with a Nicolet 6700 FTIR spectrophotometer (Thermo Fisher Scientific, Waltham, MA, USA). Nyquist plots were obtained using a three-electrode cell from 100 kHz to 10 MHz and an IM6 (Zahner Elektrik, Kronach, Germany) analyzer. Significant data were extracted from the plot using curve-fitting software (ZMAN ver. 2.3). BET surface areas were measured with an ASAP 2010 analyzer (Micrometrics, Ottawa, ON, Canada). All electrical measurements were performed with a Keithley 2612A source meter (Keithley Instruments, Inc., Cleveland, OH, USA), a probe station (model 4000; MS TECH, Arlington, VA, USA) and a Wonatech WBCS 3000 potentiostat (Wonatech, Seoul, Korea).

Acknowledgements

This research was supported by the National Research Foundation of Korea (NRF) grant funded by the Korean government (MEST) (Grant No. 2011-0017125)

Notes and references

1. Z. Altintas and I. Tothill, *Sens. Actuators B: Chem.*, 2013, **188**,

988-998.

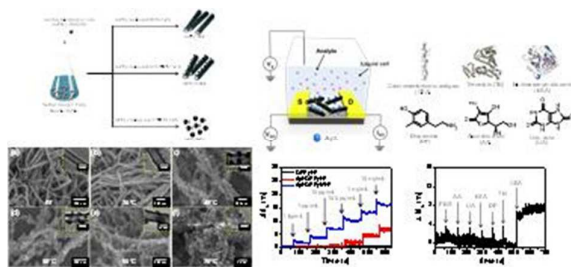
2. Z. Liu, R. Yuan, Y. Chai, Y. Zhuo, C. Hong and X. Yang, *Sens. Actuators B: Chem.*, 2008, **134**, 625-631.
3. M. Grunnet and J. B. Sorensen, *Lung Cancer*, 2012, **76**, 138-143.
4. A. M. Dela Rosa and M. Kumakura, *Anal. Chim. Acta*, 1995, **312**, 85-94.
5. T. C. Pina, I. T. Zapata, F. C. Hernández, J. B. López, P. P. Paricio and P. M. n. Hernández, *Clin. Chim. Acta*, 2001, **305**, 27-34.
6. D. Tang and J. Ren, *Anal. Chem.*, 2008, **80**, 8064-8070.
7. G. Shen and J. Lu, *Thin Solid Films*, 2010, **518**, 5010-5013.
8. Z. Altintas, Y. Uludag, Y. Gurbuz and I. E. Tothill, *Talanta*, 2011, **86**, 377-383.
9. V. Villena, A. López-Encuentra, J. Echave-Sustaeta, P. Martín-Escribano, B. Ortuño-de-Solo and J. Estenez-Alfaro, *Cancer*, 1996, **78**, 736-740.
10. D. Shitrit, B. Zingerman, A. B.-G. Shitrit, D. Shlomi and M. R. Kramer, *The Oncologist*, 2005, **10**, 501-507.
11. D. Behera, S. C. Das, V. Pathania and K. L. Khanduja, *Lung Cancer*, 1997, **18**, Supplement 1, 168.
12. T. Wang, L. Guo, C. Lei and Y. Zhou, *RSC Adv.*, 2015, **5**, 51330-51336.
13. D. Wang, Y. Li, Z. Lin, B. Qiu and L. Guo, *Anal. Chem.*, 2015, **87**, 5966-5972.
14. J. Yuan, G. Wang, K. Majima and K. Matsumoto, *Anal. Chem.*, 2001, **73**, 1869-1876.
15. J. Huang, J. Tian, Y. Zhao and S. Zhao, *Sens. Actuators B: Chem.*, 2015, **206**, 570-576.
16. D. Lin, J. Wu, H. Ju and F. Yan, *Biosens. Bioelectron.*, 2014, **52**, 153-158.
17. D. Tang and J. Ren, *Analytical Chemistry*, 2008, **80**, 8064-8070.
18. Y. Ishige, M. Shimoda and M. Kamahori, *Biosens. Bioelectron.*, 2009, **24**, 1096-1102.
19. J. Jun, J. S. Lee, D. H. Shin and J. Jang, *ACS Appl. Mater. Interfaces*, 2014, **6**, 13859-13865.
20. O. S. Kwon, S. H. Lee, S. J. Park, J. H. An, H. S. Song, T. Kim, J. H. Oh, J. Bae, H. Yoon, T. H. Park and J. Jang, *Adv. Mater.*, 2013, **25**, 4177-4185.
21. W. S. Leong, Y. Li, X. Luo, C. T. Nai, S. Y. Quek and J. T. L. Thong, *Nanoscale*, 2015, **7**, 10823-10831.
22. J. W. Park, S. J. Park, O. S. Kwon, C. Lee and J. Jang, *Anal. Chem.*, 2014, **86**, 1822-1828.
23. P. Reiss, E. Couderc, J. De Girolamo and A. Pron, *Nanoscale*, 2011, **3**, 446-489.
24. S. Chen and G. Sun, *ACS Appl. Mater. Interfaces*, 2013, **5**, 6473-6477.
25. J. I. Lee, S. H. Cho, S.-M. Park, J. K. Kim, J. K. Kim, J.-W. Yu, Y. C. Kim and T. P. Russell, *Nano Letters*, 2008, **8**, 2315-2320.
26. S. Park, S. An, H. Ko, C. Jin and C. Lee, *ACS Appl. Mater. Interfaces*, 2012, **4**, 3650-3656.
27. L. Wang, J. Deng, Z. Lou and T. Zhang, *J. Mater. Chem. A*, 2014, **2**, 10022-10028.
28. H. Yoon, S. H. Lee, O. S. Kwon, H. S. Song, E. H. Oh, T. H. Park and J. Jang, *Angew. Chem. Int. Ed.*, 2009, **48**, 2755-2758.
29. P. Lu and A. V. Walker, *ACS Nano*, 2009, **3**, 370-378.
30. J. Luo, L. Ma, T. He, C. F. Ng, S. Wang, H. Sun and H. J. Fan, *J. Phys. Chem. C*, 2012, **116**, 11956-11963.
31. B. Shukla, T. Saito, S. Ohmori, M. Koshi, M. Yumura and S. Iijima, *Chem. Mater.*, 2011, **23**, 1636-1636.
32. C. M. Cobley, J. Chen, E. C. Cho, L. V. Wang and Y. Xia, *Chem. Soc. Rev.*, 2011, **40**, 44-56.
33. P. Y. Keng, M. M. Bull, I.-B. Shim, K. G. Nebesny, N. R. Armstrong, Y. Sung, K. Char and J. Pyun, *Chem. Mater.*, 2011, **23**, 1120-1129.
34. L. Jiang, S. Yinghui, H. Peng, L.-J. Li, T. Wu, J. Ma, F. Y. Chiang Boey, X. Chen and L. Chi, *Small*, 2011, **7**, 1949-1953.
35. H. D. Tran, D. Li and R. B. Kaner, *Adv. Mater.*, 2009, **21**, 1487-1499.
36. Z. Yin and Q. Zheng, *Adv. Energy Mater.*, 2012, **2**, 179-218.
37. C. Li, H. Bai and G. Shi, *Chem. Soc. Rev.*, 2009, **38**, 2397-2409.
38. S. Bai, C. Sun, P. Wan, C. Wang, R. Luo, Y. Li, J. Liu and X. Sun, *Small*, 2015, **11**, 306-310.
39. H. Yoon, J.-Y. Hong and J. Jang, *Small*, 2007, **3**, 1774-1783.
40. J. S. Lee, J. Oh, S. G. Kim and J. Jang, *Small*, 2015, **11**, 2399-2406.
41. M. E. Alf, A. Asatekin, M. C. Barr, S. H. Baxamusa, H. Chelawat, G. Ozaydin-Ince, C. D. Petruczuk, R. Sreenivasan, W. E. Tenhaeff, N. J. Trujillo, S. Vaddiraju, J. Xu and K. K. Gleason, *Adv. Mater.*, 2010, **22**, 1993-2027.
42. A. Laforgue and L. Robitaille, *Chem. Mater.*, 2010, **22**, 2474-2480.
43. S. Nair, E. Hsiao and S. H. Kim, *Chem. Mater.*, 2009, **21**, 115-121.
44. N. J. Trujillo, M. C. Barr, S. G. Im and K. K. Gleason, *Journal of Materials Chemistry*, 2010, **20**, 3968-3972.
45. O. S. Kwon, J.-Y. Hong, S. J. Park, Y. Jang and J. Jang, *J. Phys. Chem. C*, 2010, **114**, 18874-18879.
46. H. Yoon, M. Chang and J. Jang, *Adv. Funct. Mater.*, 2007, **17**, 431-436.
47. D. Tingyang, Y. Xiaoming and L. Yun, *Nanotechnology*, 2006, **17**, 3028.
48. X. Yang, Z. Zhu, T. Dai and Y. Lu, *Macromol. Rapid Commun.*, 2005, **26**, 1736-1740.
49. O. S. Kwon, S. J. Park, H.-W. Park, T. Kim, M. Kang, J. Jang and H. Yoon, *Chem. Mater.*, 2012, **24**, 4088-4092.
50. O. S. Kwon, S. J. Park, H. Yoon and J. Jang, *Chem. Commun.*, 2012, **48**, 10526-10528.
51. S. Bose, T. Kuila, M. E. Uddin, N. H. Kim, A. K. T. Lau and J. H. Lee, *Polymer*, 2010, **51**, 5921-5928.
52. J. W. Park, C. Lee and J. Jang, *Sens. Actuators B: Chem.*, 2015, **208**, 532-537.
53. Z. Wu, H. Li and Z. Liu, *Sens. Actuators B: Chem.*, 2015, **206**, 531-537.
54. K. F. Chan, H. N. Lim, N. Shams, S. Jayabal, A. Pandikumar and N. M. Huang, *Mater. Sci. Eng. C*, 2016, **58**, 666-674.
55. J. Huang, J. Tian, Y. Zhao and S. Zhao, *Sens. Actuators B: Chem.*, 2015, **206**, 570-576.
56. X. Yang, Y. Zhuo, S. Zhu, Y. Luo, Y. Feng and Y. Xu, *Biosens. Bioelectron.*, 2015, **64**, 345-351.
57. K. Liang, S. Zhai, Z. Zhang, X. Fu, J. Shao, Z. Lin, B. Qiu and G.-n. Chen, *Analyst*, 2014, **139**, 4330-4334.
58. Z.-M. Zhou, Z. Feng, J. Zhou, B.-Y. Fang, Z.-Y. Ma, B. Liu, Y.-D. Zhao and X.-B. Hu, *Sens. Actuators B: Chem.*, 2015, **210**, 158-164.
59. Z.-M. Zhou, J. Zhou, J. Chen, R.-N. Yu, M.-Z. Zhang, J.-T. Song and Y.-D. Zhao, *Biosens. Bioelectron.*, 2014, **59**, 397-403.
60. G. Zheng, F. Patolsky, Y. Cui, W. U. Wang and C. M. Lieber, *Nat Biotech.*, 2005, **23**, 1294-1301.

Journal Name

ARTICLE

61. X. Fu, R. Huang, J. Wang and B. Chang, *RSC Adv.*, 2013, **3**, 13451-13456.
62. L. Li, C. Ma, Q. Kong, W. Li, Y. Zhang, S. Ge, M. Yan and J. Yu, *J. Mater. Chem. B*, 2014, **2**, 6669-6674.
63. X. Wang, C. Chu, L. Shen, W. Deng, M. Yan, S. Ge, J. Yu and X. Song, *Sens. Actuators B: Chem.*, 2015, **206**, 30-36.
64. X. Zeng, S. Ma, J. Bao, W. Tu and Z. Dai, *Anal. Chem.*, 2013, **85**, 11720-11724.

Graphic abstract (80 mm broad × 37 mm high)



The aptamer FET sensors based on carboxylated polypyrrole multidimensional nanotubes show ultrahigh sensitivity and selectivity toward CEA, and superior lifetime.